Acta Cryst. (1999). A**55**, 188–196

Three-phase structure invariants and structure factors determined with the quantitative convergent-beam electron diffraction method

R. Høier,[a]* C. R. Birkeland,[a] R. Holmestad[a] and K Marthinsen[b]

[a]*Department of Physics, and* [b]*Department of Metallurgy, Norwegian University of Science and Technology (NTNU), N-7034 Trondheim, Norway. E-mail: ragnvald.hoier@phys.ntnu.no*

(*Received 21 January 1998; accepted 29 June 1998*)

Dedicated to Professor A. F. Moodie on the occasion of his 75th birthday

Abstract

Quantitative convergent-beam electron diffraction is used to determine structure factors and three-phase structure invariants. The refinements are based on centre-disc intensities only. An algorithm for parameter-sensitive pixel sampling of experimental intensities is implemented in the refinement procedure to increase sensitivity and computer speed. Typical three-beam effects are illustrated for the centrosymmetric case. The modified refinement method is applied to determine amplitudes and three-phase structure invariants in noncentrosymmetric InP. The accuracy of the results is shown to depend on the choice of the initial parameters in the refinement. Even unrealistic starting assumptions and incorrect temperature factor lead to stable results for the structure invariant. The examples show that the accuracy varies from 1 to 10° in the electron three-phase invariants determined and from 0.5 to 5% for the amplitudes. Individual phases could not be determined in the present case owing to spatial intensity correlations between phase-sensitive pixels. However, for the three-phase structure invariant, stable solutions were found.

1. Introduction

Determination of structure-factor phases is a classical problem in structure studies. This is because intensities and thus only the amplitudes are found experimentally. In traditional X-ray structure determination, this problem is coped with by using probabilistic estimates based on intensities, and direct methods have a long tradition (*e.g.* Giacovazzo, 1980). In electron crystallography, these methods have not until relatively recently been used, primarily due to multiple scattering and dynamical effects (Dorset, 1995). However, it has long been known that phase information can be obtained both from three-beam electron diffraction effects (Kambe, 1957; Gjønnes & Høier, 1971; Ichimiya & Uyeda, 1977; Hurley & Moodie, 1980) and from single-crystal *Pendellösung* X-ray work (Hart & Lang, 1961; Høier & Aanestad, 1981; Høier & Marthinsen, 1983). Similar effects have also been discussed in electron channelling patterns (Marthinsen & Høier, 1986, 1988). Concerning experimental phases, the X-ray field has changed considerably over the last 15–20 years. The methodology has been extended to also include three-phase structure invariants determined from observed three-beam intensity profiles. The field of three-beam X-ray studies has been reviewed by Chang (1987) and Weckert & Hümmer (1997). Recent results can be found in papers by *e.g.* Mathiesen *et al.* (1998), Shen (1998) and theoretical work by Larsen & Thorkildsen (1998).

The present investigation concerns phase determination with electron-based methods. In electron diffraction, the scattering is much stronger than with X-rays. Hence, dynamical effects depending on both structure-factor magnitudes and phases are more pronounced and easily observed. This is in particular the case in convergent-beam electron diffraction (CBED) and also in Kikuchi-line patterns, as shown in studies by *e.g.* Kambe (1957), Goodman & Lehmpfuhl (1967), Watanabe *et al.* (1968), Gjønnes & Høier (1969, 1971), Høier (1972), Høier & Andersson (1974), Hurley & Moodie (1980), Fox & Fisher (1988), Zuo, Høier & Spence (1989), Høier *et al.* (1993), Spence (1998), Holmestad *et al.* (1999) and Zuo (1999). A review is given by Spence (1993); see also Spence & Zuo (1992).

In addition to strong scattering obtained with electrons, the electron spot in CBED can be focused down to nanometer-sized regions. Typically, the volume investigated with electrons may be of several orders of magnitude smaller than in X-ray crystallography. Consequently, the crystal mosaicity in X-ray experiments can be avoided by investigating defect-free crystallites selected by direct observation in electron microscopy. Further, as the incident beam can be considered to be a plane wave in the electron diffraction case, while one has spherical X-ray waves, broadening of the experimental intensity profiles owing to convolution effects are strong with X-rays but negligible with electrons.

Today, the principles for taking dynamical and absorption effects into account are well developed (see *e.g.* Spence & Zuo, 1992) and the field of quantitative convergent-beam electron diffraction (QCBED) is

ISSN 0108-7673

growing rapidly. At present, parameters are determined with high accuracy, in particular the structure-factor amplitude. This amplitude is determined with an accuracy down to a few tenths of a percent, while about one tenth of a degree has been found for an X-ray phase calculated from the corresponding electron phase (see *e.g.* Bird *et al.*, 1987; Zuo *et al.*, 1988, Zuo, Spence & Høier, 1989; Saunders *et al.*, 1995; Høier *et al.*, 1993; Zuo *et al.*, 1993; Tomokiyo *et al.*, 1993; Holmestad *et al.*, 1995; Zuo *et al.*, 1997; Nüchter *et al.*, 1998, and references therein). Further, the large majority of the diffraction effects utilized to obtain structure-factor information, amplitudes as well as phases, can be understood on the basis of a few beams only (Gjønnes & Høier, 1971; Høier, 1972; Hurley & Moodie, 1980; Marthinsen *et al.*, 1988; Zuo, Høier & Spence, 1989; Moodie *et al.*, 1996).

In the present studies, we focus on the possibility of extracting phase information from electron diffraction experiments in the growing field of electron crystallography. Emphasis is on diffraction and more specifically on quantitative results from the convergent-beam technique. Kikuchi-line diffraction patterns have similarities to CBED concerning many-beam effects, and phase information can be extracted with this technique as well. The typical three-beam expressions are illustrated below by examples from centrosymmetric Si. However, emphasis in the present studies is on determination of structure factors and phase invariants in noncentrosymmetric InP. For this, a new simulation procedure is developed and the dependency of the parameters refined on the accuracy of the initial data set is investigated in detail. The experimental data are taken from the centre disc only. The aim is to test out the potential use of this complicated two-dimensional intensity distribution as experimental base in QCBED investigations. Parameter-sensitive pixel sampling is applied in all refinements.

2. Theory

The intensity of the electron diffraction patterns is calculated from the standard Bloch-wave formulation of the dynamical theory (Spence & Zuo, 1992). The crystal is described by a periodic potential $V(\mathbf{r})$ and the solutions of the wave function are in Bloch form. Conventionally, we introduce

$$U(\mathbf{r}) = (2me/h^2)V(\mathbf{r}), \tag{1}$$

where

$$U(\mathbf{r}) = \sum_h U_h \exp(2\pi i \mathbf{h}\cdot\mathbf{r}) \tag{2}$$

and

$$U_h = |U_h| \exp(i\varphi_h). \tag{3}$$

The Fourier coefficients of $U(\mathbf{r})$, U_h, are termed structure factors for electrons. From the Schrödinger equation, we get the following intensity in a Bragg beam **g**:

$$I_g = |\Psi_g|^2 = \left|\sum_i \alpha^i C_g^i \exp(2\pi i \mathbf{k}_g\cdot\mathbf{r} + \gamma^i z)\right|^2. \tag{4}$$

Here C_g^i is an eigenvector component and γ^i an eigenvalue equal to the change in wavevector along the surface normal at the entrance surface. γ^i is a function of the structure factors U_g and the deviations from the Bragg condition expressed by the excitation errors s_g. α^i is a normalization factor equal to C_0^{i*} for the Hermitian case and C_0^{-1} otherwise.

In our discussion of phase information, we focus on cases that involve more than two beams with geometry in reciprocal space being a nonsystematic sparse zone axis as shown schematically in Fig. 1, where the three-beam case **0**, **g** and **h** is shown. The structure-factor phases involved in this case are φ_g, φ_{g-h} and φ_h. The corresponding reciprocal vectors form a closed loop and for this case it is easily shown (*e.g.* Giacovazzo, 1980) that the following phase sum is independent of the position chosen as origin in the crystal unit cell:

$$\psi = \varphi_h - \varphi_g + \varphi_{g-h}. \tag{5}$$

ψ is the three-phase structure invariant (or the triplet phase). In determination of phases, this invariant is as a rule the quantity referred to in previous experimental and theoretical electron diffraction studies (Kambe, 1957; Gjønnes & Høier, 1969, 1971; Høier, 1972; Hurley & Moodie, 1980; Moodie *et al.*, 1996). Determination of the individual phases from diffraction have been discussed by *e.g.* Ichimiya & Uyeda (1977), Bird *et al.* (1987), Zuo, Høier & Spence (1989), Zuo *et al.* (1993), Cheng *et al.* (1996) and Spence (1998). The eigensystem is solved in the usual way by inserting a periodic potential and Bloch waves in the Schrödinger equation, see Spence & Zuo (1992).

The three-beam equation for the eigenvalue becomes (Marthinsen *et al.*, 1988)

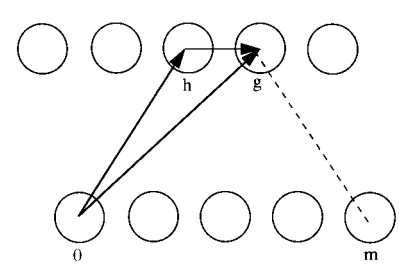

Fig. 1. Example of sparse zone axis with the four-beam case 0, **g**, **h**, **m**.

$$(2K\gamma)^3 - (2K\gamma)^2(2Ks_g + 2Ks_h) + 2K\gamma(4K^2 s_h s_g - |U_g|^2 - |U_h|^2 - |U_{g-h}|^2) + 2Ks_h|U_g|^2 + 2Ks_g|U_h|^2 - 2|U_g||U_h||U_{h-g}|\cos\psi = 0. \quad (6)$$

This equation shows the important result that the eigenvalues γ^i only depend on the three-phase structure invariant ψ and not on the individual structure-factor phases, φ_h. The same is of course also true for deduced quantities like the dispersion-surface gap at the Brillouin-zone boundaries and the corresponding proportional quantity defined as the effective potential, $U_g^{\rm eff}$ (Zuo, Høier & Spence, 1989). By dispersion-surface gap in this three-beam case, we mean the perturbed two-beam gap associated with a Bragg beam **h** in the presence of a coupled beam **g** with coupling constant U_{g-h}.

For a crystal with centrosymmetry, the phase invariant ψ is either 0 or 180°. For a particular incident-beam direction, it has been shown in this case that the eigenvalue equation has a degeneracy between the two solutions for γ that correspond to the two-beam case (Gjønnes & Høier, 1971). This degeneracy is found for all centrosymmetric three-beam cases, independent of the acceleration voltage of the microscope. This particular incident-beam direction is characterized by the following excitation error values:

$$2Ks_g^{\rm crit} = |U_g|(|U_{g-h}|^2 - |U_h|^2)/|U_h||U_{g-h}|\cos\psi,$$
$$2Ks_h^{\rm crit} = |U_h|(|U_{g-h}|^2 - |U_g|^2)/|U_g||U_{g-h}|\cos\psi. \quad (7)$$

In practice, these excitation errors can easily be determined from the positions of the degeneracy point in the diffraction pattern. Thus, both their magnitude and sign give structure-factor information as shown below. Through this point in the s_g, s_h plane, it has also been shown that the dispersion equation can be solved along special lines (Moodie *et al.*, 1996). Along these, the intensity expression is of two-beam form as one of the dispersion-surface branches is not excited.

Simple expressions to interpret and understand many-beam effects have been suggested. Two central approximations for including the effects of additional beams in a two-beam formalism are due to Kambe (1957) and Bethe (1928), see discussion by Zuo, Høier & Spence (1989).

3. Dynamical effects in centrosymmetric Si

Typical three-beam effects are most easily identified in centrosymmetric crystals. A sparse zone-axis pattern from Si not too far from the major zone axis [1$\bar{1}$1] is

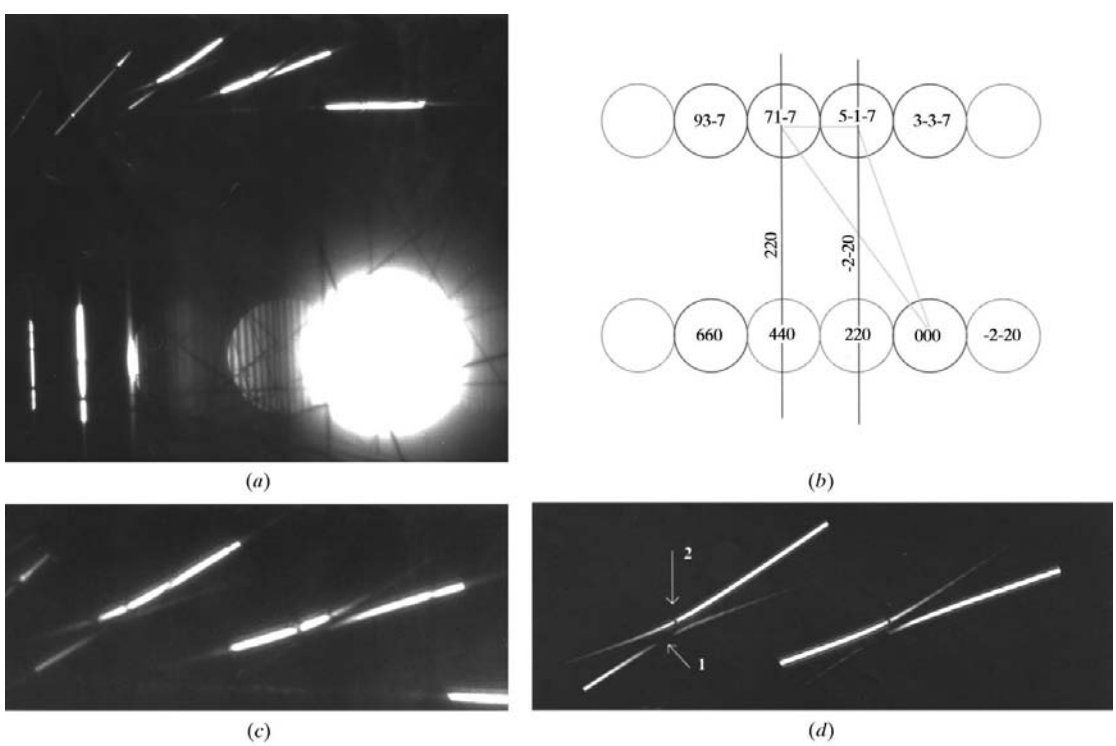

Fig. 2. (*a*) Experimental CBED pattern from Si, near the [1$\bar{1}$1] zone axis. (*b*) Indexed pattern. (*c*) 71$\bar{7}$ and 5$\bar{1}\bar{7}$ discs from experimental pattern. (*d*) 71$\bar{7}$ and 5$\bar{1}\bar{7}$ discs calculated with the four beams 000, 71$\bar{7}$, 5$\bar{1}\bar{7}$, 660. 1 indicates the intensity minimum corresponding to the position of the degeneracy point. 2 indicates the position of the gap between the hyperbolae, proportional to the coupling reflection U_{g-h}.

shown in Fig. 2(*a*) and the corresponding indexing in Fig. 2(*b*). Figs. 2(*c*) and (*d*) show experiment and calculation of the two discs $5\bar{1}\bar{7}$ and $71\bar{7}$ using four beams only. The fourth beam is included owing to symmetry. It influences the pattern only with the narrow minimum at the gap position (arrow 2). The agreement between Figs. 2(*c*) and (*d*) is qualitatively very good. This Si pattern was taken on film in a Philips CM30 electron microscope operated at 300 kV at liquid-N_2 temperature. The horizontal axis is the systematic 220 row and the specimen is tilted so that the midpoint of the centre disc represents the four-beam case 000, $5\bar{1}\bar{7}$, $71\bar{7}$, 660. We focus on the first three reflections **0**, **g**, **h**. The two reflections **g** and **h** are weak and the coupling reflection relatively strong. Near their intersection, the **g** and **h** lines are seen to be split into hyperbolae in accordance with theory and weak thickness fringes are seen. The gap between the hyperbolae that is indicated in Fig. 2(*d*) is proportional to the coupling reflection U_{g-h}. The intensity is seen to decrease continuously along the lower hyperbola towards the degeneracy point (arrow 1). Here it is not defined as pointed out by Moodie *et al.* (1996). The measurable excitation errors s_g and s_h at this point couple directly to the structure-factor amplitudes and three-phase invariant through (7). This use of the dynamical effect for structure-factor determination is called the intersecting-Kikuchi-line (IKL) method (Gjønnes & Høier, 1971) and the corresponding method for high-order Laue-zone (HOLZ) lines is the intersecting-HOLZ-line (IHL) method. By inspection, both s_g and s_h are seen to be positive and the phase invariant becomes $\psi = 0$ as expected for all invariants in Si. By systematic tilting to the similar neighbouring three-beam cases, and also to other sparse zones, a number of invariants can be found experimentally without any calculations in these strong coupling cases. It should be noted that the effects are in principle always present, visible or not, depending on the magnitude of the three structure factors involved.

4. Experimental and numerical data for InP

CBED patterns from the noncentrosymmetric crystal InP have been acquired in a Leo 912 microscope equipped with an Omega energy filter. The experimental pattern shown in Fig. 3(*a*) is recorded at liquid-N_2 temperature with a slow-scan CCD camera. In the refinements, an accurate microscope voltage is essential. It has been determined to 119.5 (1) kV using the method of Zuo (1992). The specimen is tilted close to the $[\bar{1}\bar{7}0]$ zone such that the diffraction geometry is the same as the one for silicon above. Alternatives to this sparse-zone-axis geometry are the low-index zone axis (Saunders *et al.*, 1995) and the systematic row geometry (Spence & Zuo, 1992). Among these, the latter geometry has been most used in QCBED so far.

In the simulations, the theoretical intensities I_i^{theory} are calculated from dynamical theory diagonalizing on average 20 beams and including 164 additional beams using Bethe perturbations (Fig. 3*b*). The beam-selection criteria are taken from Birkeland *et al.* (1996). Initial structure-factor values are determined for neutral atoms using the algorithm of Bird & King (1990). Debye–Waller factors given by Reid (1983) are used, *i.e.* $B_{\text{In}} = 0.3226$ and $B_{\text{P}} = 0.2652$ Å^2. Theoretical corections have recently been given by Anstis (1996). The thickness is included in all refinements of structural parameters with non-essential variations in the refined value from case to case. Typically, it is 1400 Å.

The CBED pattern acquired includes a systematic 002 row of reciprocal-lattice points and a parallel row of type $7\bar{1}(2n+1)$, *i.e.* the diffraction geometry in Fig. 1. The incident-beam direction represented by the centre of the zero disc corresponds to the 000, $7\bar{1}3$, $7\bar{1}5$, 008 four-beam condition. If we focus on three-beam effects, both the 000, $7\bar{1}3$, $7\bar{1}5$ and the 000, $7\bar{1}1$, $7\bar{1}5$ cases are seen within the CBED discs. The experimental centre disc and the indexing of the HOLZ lines are shown in Figs. 3(*a*) and (*c*), respectively. A corresponding InP example of using the two-dimensional intensity distribution in Bragg discs for systematic structure-factor determination is reported by Høier *et al.* (1993). The refinements in this work are based on the intensity of this centre disc only. Earlier quantitative work has often been based on intensity in Bragg discs combined with the centre disc. Use of only the centre disc has as a rule been considered too complicated for practical use. This is due to many HOLZ lines and heavy line overlap as seen in Fig. 3(*a*). However, the information content in the pattern is large. To extract this information, the time-consuming simulations needed can be reduced if one can single out the parameter-sensitive pixels in the disc, from now called the window function W_i.

To arrive at accurate structure-factor values, the strategy in the quantitative CBED method is to compare the experimental and corresponding calculated pattern pixel by pixel and minimize a goodness-of-fit parameter:

$$\chi^2 = \frac{1}{(n-m-1)} \sum_{i=1}^{n} \frac{W_i[I_i^{\text{exp}} - cI_i^{\text{theo}}(a_1 \ldots a_m) - B]^2}{\sigma_i^2}, \tag{8}$$

where I_i^{exp} and I_i^{theo} are experimental and theoretical intensities, respectively, σ_i is the corresponding standard deviation, n is the number of pixels in the pattern, a_1 to a_m are the m unknown refined parameters, c is a normalization constant, B the background and W_i a window function.

Use of χ^2 in QCBED has recently been discussed in detail by Holmestad & Birkeland (1998). In particular, they address cases where the χ^2 value is much larger than one, indicating that the model is wrong or that the measurement errors are larger than asssumed. To

understand these cases, they point at the assumptions used to define χ^2: (i) the uncertainties σ_i associated with the experimental intensities $I_i^{\rm exp}$ are known; and (ii) the theoretical intensities $I_i^{\rm theo}$ are known exactly. Only if both these assumptions are fulfilled can the χ^2 values be used quantitatively to evaluate how accurate the fit and the refined parameters are. Otherwise, the fit factor should only be regarded as a tool to find the best match and to refine theoretical parameters.

Often in QCBED and in particular in the present investigation, neither of the assumptions are strictly fulfilled. In general, there are a number of effects that may contribute to larger χ^2 values. The Debye–Waller factor for example is usually taken to be isotropic and is often not accurately known. Further, only a few parameters are simultaneously refined and the modelling of the background is in most cases oversimplified, in particular for thicker crystals, see Holmestad & Birkeland (1998). In the experiments to be discussed below, the intensities are taken from the centre disc only. This two-dimensional intensity distribution with its rapidly varying contrast is much more involved than the distribution in Bragg discs usually used in other QCBED methods. The absorption effects may be pronounced and Kikuchi lines are frequently observed in the background except for the case of very thin crystals. Although coefficients of the absorptive potential may be calculated, they are usually underestimated. In general, χ^2 values have also been found to increase with increasing crystal thickness (Nuchter *et al.*, 1998).

In the minimization, the relevant parameters are systematically varied and refined in a least-squares multiparameter algorithm (Press *et al.*, 1986). The global minimum defines the final parameter set (Marthinsen *et al.*, 1990; Spence & Zuo, 1992; see also Zuo, 1999). This method is used in all refinements below. The first step is to determine the incident-beam direction. As the second

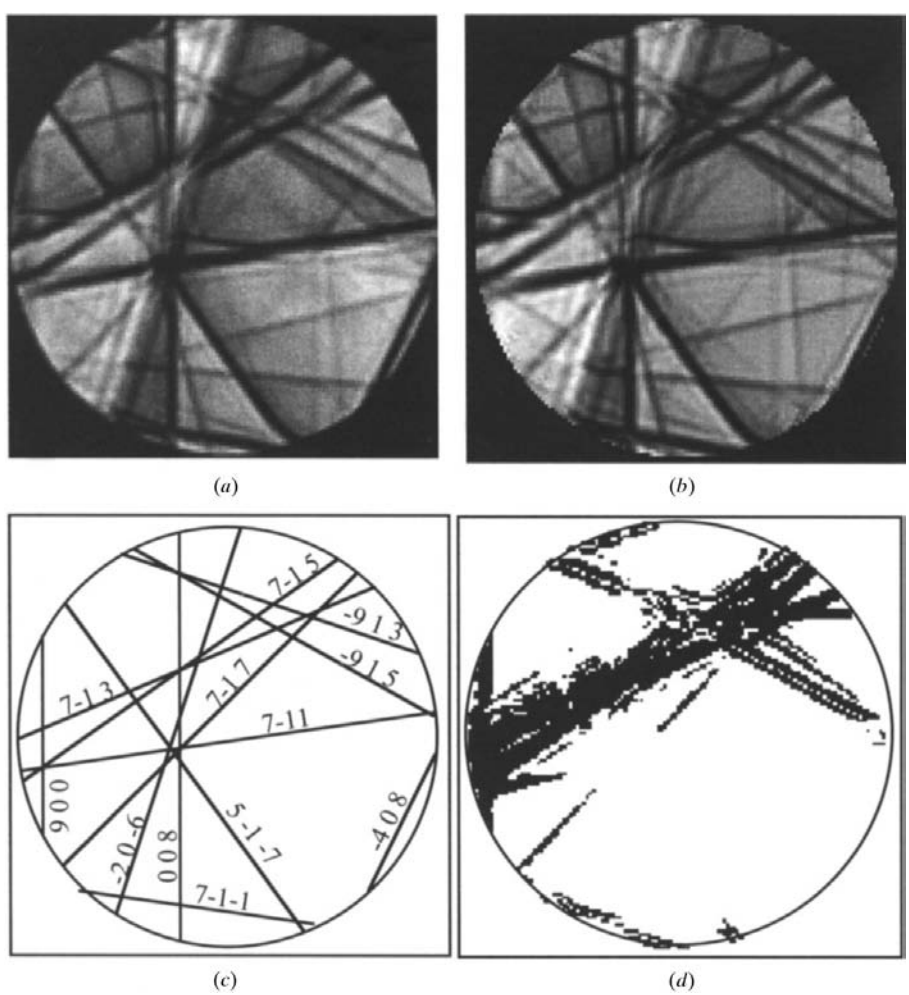

Fig. 3. (*a*) Centre disc of the experimental CBED pattern of InP near the [1$\bar{7}$0] zone axis. (*b*) Simulated theoretical pattern. Note the excellent match in grey scales with (*a*). (*c*) Indexed centre disc. (*d*) Window function used in pixel-sensitive QCBED procedure.

Table 1. *Results of the refinement procedure; structure-factor amplitudes and phases, the three-phase structure invariant* $\psi = \varphi_{7\bar{1}5} - \varphi_{7\bar{1}3} + \varphi_{002}$ *and* χ^2 *values for selected refinements*

Run	Description	U_{002}	$U_{7\bar{1}3}$	$U_{7\bar{1}5}$	$\varphi_{7\bar{1}3}$ (°)	$\varphi_{7\bar{1}5}$ (°)	Ψ (°)	χ^2
1	Neutral atom values	0.023288	0.011116	0.008923	19.58	−19.88	39.46	48.4
	Refined values	0.023334	0.010920	0.008322	–	–	–	47.5
2	Start values	0.023288	0.011116	0.008923	19.58	45.88	−26.3	77.0
	Refined values	0.023331	0.010873	0.008298	–	−20.73	40.31	47.4
3	Start values	0.023288	0.011116	0.008923	65.00	65.00	0.00	117.4
	Refined values	0.023393	0.010845	0.008352	23.10	−16.58	39.68	47.5
4	Start values	0.025	0.013	0.011	0.00	−19.88	19.88	79.4
	Refined values	0.023411	0.010951	0.008297	20.44	–	40.32	47.4

step, we now introduce a new algorithm to determine the window function W_i.

5. Refinement for InP – standard structure-factor initial values

5.1. *Refinement of the incident-beam direction*

Figs. 3(*a*) and (*c*) show the experimental CBED pattern with indexing. The incident-beam direction can first be found approximately using the software *Ideal Microscope* (Zhu & Zuo, 1993). This is the basis of a refinement where the incoming-beam direction is varied until the best match between theoretical calculations and the experiment is found. Because the pattern consists of many sharp HOLZ lines, the best match is well defined and the procedure used is robust. The incoming-beam direction is determined with great accuracy. Figs. 3(*a*) and (*b*) show the experimental and the simulated image, respectively. Note that all HOLZ lines are properly reproduced and that grey scales match almost perfectly. This is the first step in the QCBED procedure.

5.2. *Parameter-sensitive pixel sampling*

This new method is introduced to increase the sensitivity of the QCBED algorithm. The principle is to identify the limited areas of the CBED pattern that are sensitive to the parameters refined (Birkeland *et al.*, 1997). In this way, pixels without information are neglected and the computer time reduced. The goodness of fit, given in (8), is used. This definition includes a window function W_i containing the sensitive pixels for the relevant parameters. After the initial incident-beam-direction refinement, a step-by-step description of the method for determining W_i is:

(i) With fixed incoming-beam direction, calculate a theoretical reference image using the initial input values of the parameters $(a_1, \ldots, a_m)$.

(ii) Calculate new theoretical images after perturbing the parameters $(a_1, \ldots, a_m)$. A one-parameter-at-a-time procedure is suggested as this helps in identifying correlation effects between different parameters.

(iii) Calculate difference maps between images calculated in steps (i) and (ii). For each parameter, these maps are plotted to determine how each parameter affects the total CBED pattern.

(iv) A threshold value is set for each pixel i in the pattern. If the difference-map intensity is higher than the threshold, set $W_i = 1$, else disregard pixel i ($W_i = 0$). Repeating this for all difference maps gives a set of different window functions W_i. The union of these window functions W_i is used in the refinements.

5.3. *Discussion*

The aim is to determine the structure-factor amplitudes U_{002}, $U_{7\bar{1}3}$ and $U_{7\bar{1}5}$, the corresponding phases $\varphi_{7\bar{1}3}$ and $\varphi_{7\bar{1}5}$ and the three-phase invariant ψ. These reflections are seen in the centre disc shown in Fig. 3(*a*). The QCBED algorithm described is used to generate the window function that identifies the parameter-sensitive pixels. This window is shown in Fig. 3(*d*). Note that most points are found close to the crossing of the $7\bar{1}3$ and $7\bar{1}5$ HOLZ lines where the effects of the dynamical coupling are strongest.

InP has a known f.c.c. crystal structure. Indium is taken to be at the origin and the neutral-atom structure-factor phases are $\varphi_{002} = 0.0$, $\varphi_{7\bar{1}3} = 19.58$ and $\varphi_{7\bar{1}5} = -19.88°$. The corresponding three-phase structure invariant is $\psi = 39.5°$. The refinement procedure is repeated for various initial starting structure-factor amplitudes and phases. The results are summarized in Table 1. In run 1, only the three structure-factor amplitudes are refined and the result is used as a reference in subsequent runs. The refinements were performed for a wide range of initial starting values. Three of the runs are listed in Table 1. The large difference between the initial χ^2 values and the final ones illustrates the sensitivity of the method. Final values of χ^2 are relatively large (see discussion in §4), but as all the refinements seem to end in the same minimum one can still have confidence in the results. This is also supported by *ab initio* calculations using the FLAPW (full linear potential augmented plane-wave) method (Blaha, Schwarz & Augustyn, 1990; Blaha, Schwarz, Sorantin & Triskey, 1990). For example, for U_{002}, these calculations give a small positive change from the neutral-atom value in accordance with the results in Table 1. An analysis of the table shows that the

Table 2. *Fit factors after QCBED refinements using approaches (A), (B) and (C) defined in the text*

χ_1^2 is the best match after refining the incoming-beam direction only. χ_2^2 refers to the best fit factor after refinement of beam direction and five structure-factor amplitudes.

Run	χ_1^2	χ_2^2
(*A*)	54.2	49.2
(*B*)	276	84.9
(*C*)	175	58.3

three-phase structure invariant can be determined with an accuracy of approximately 1° in this case. Also, assuming that the structure-factor amplitudes found in run 1 are accurate, all refinements determine the structure-factor amplitudes with an accuracy better than 0.5%

Table 3. *Results of structure-factor amplitude refinements using assumptions (A), (B) and (C) defined in the text*

g		Neutral U_g	Refined U_g	Error
002	(*A*)	0.02329	0.02309	
	(*B*)	0.07352	0.02306	−0.1%
	(*C*)	0.04845	0.02259	−2.2%
004	(*A*)	0.03693	0.03353	
	(*B*)	0.03717	0.03444	+2.7%
	(*C*)	0.02647	0.03195	−4.7%
006	(*A*)	0.01007	0.00936	
	(*B*)	0.02158	0.01157	+23.6%
	(*C*)	0.01596	0.00901	−3.7%
008	(*A*)	0.01321	0.01256	
	(*B*)	0.01357	0.01613	+28.4%
	(*C*)	0.01007	0.01249	−0.6%
$\bar{2}0\bar{6}$	(*A*)	0.01959	0.02291	
	(*B*)	0.01992	0.02895	+26.4%
	(*C*)	0.01477	0.02241	−2.2%

6. Refinement with inaccurate initial structure-factor values

6.1. *Assumptions*

To test the influence of inaccurate initial input data on the QCBED results, a hypothetical unknown noncentrosymmetric crystal is defined. The same experimental pattern as in §5 is used. The assumed preknowledge from other methods is: The crystal has a cubic face-centred lattice with known lattice parameters and density and a unit cell consisting of the two atom types In and P, with equal atomic percentage. Three approaches are taken regarding atomic positions in the unit cell:

(*A*) As a reference, we use the known InP f.c.c. structure with the heaviest atom In at the origin and P at $(\frac{1}{4}, \frac{1}{4}, \frac{1}{4})$.

(*B*) We assume that one In and one P atom are superimposed on the f.c.c. positions. This is not a realistic approach but it ensures that the total number of atoms in the unit cell is correct. The cell is centrosymmetric.

(*C*) As the atomic number of In (49) is much larger than P (15), only the heavy In atoms are included in the basis, *i.e.* a hypothetical centrosymmetric f.c.c. crystal is assumed.

With these three structure models, initial structure-factor values are determined using the algorithm of Bird & King (1990). It should be noted that the second approach (*B*) is expected to overestimate the diffraction effects and dynamical interactions as the initial structure factors will be equal or larger than in InP. Approach (*C*) may be more reasonable but the total lack of P atoms is not intuitively satisfying.

Both the approaches (*B*) and (*C*) give a centrosymmetric crystal, with all elastic structure-factor phases initially equal to zero. However, it should be stressed that these crude assumptions are used only to provide a set of starting values and that important parameters are adjusted in the following refinement procedure. However, the nonrefined initial structure factors are the same during the refinement and this contributes to the methodical errors. Another question is the estimation of Debye–Waller factors. For approach (*A*), the Debye–Waller factors given by Reid are used, *i.e.* $B_{\rm In} = 0.3226$ and $B_{\rm P} = 0.2652$ Å. For cases (*B*) and (*C*), we take the temperature factors $B_{\rm In} = B_{\rm P} = 0.25$ Å, a typical value for similar crystals at liquid-N_2 temperature.

Both the approximations (*B*) and (*C*) are compared with the known structure, case (*A*). The observed pattern is indexed (see Fig. 3*b*) and the reflections to be included in the calculations are selected. A natural approach is to include all the reflections seen in the centre disc, in this case 25 (§3), including the direct 000 beam and the strongly dynamical 002 and 004 beams.

With these assumptions [(*B*) and (*C*)], the model is intentionally chosen to be wrong in order to test the robustnes of the refinement procedure.

6.2. *Determining the incident-beam direction and selected structure-factor amplitudes*

The χ^2 procedure was applied to determine the incident-beam direction for all the three assumptions (*A*), (*B*) and (*C*), and the results are given by χ_1^2 in Table 2. The fit is not good for (*B*) and (*C*), which is also easily seen by a visual comparison. For the simulations based on assumptions (*B*) and (*C*), a careful comparison with the experimental image (Fig. 3*a*) shows a large mismatch near the $7\bar{1}3$ and $7\bar{1}5$ crossing. The gap between the $7\bar{1}3$ and $7\bar{1}5$ lines is much too wide in the simulated patterns. From three-beam theory, this gap is proportional to the coupling between the two beams. In this case, this indicates that the 002 structure factor is wrong in the simulations. Therefore, the refinement of the incident-beam direction was repeated but this time allowing the 002 structure factor to vary freely giving a much better

Table 4. *Results of the three-phase invariant refinements using methods (A), (B) and (C)*

Method	χ^2	$\varphi_{7\bar{1}3}$ (°)	$\varphi_{7\bar{1}5}$ (°)	$\varphi_{7\bar{1}7}$ (°)	Ψ_1 (°)	Ψ_2 (°)	Ψ_3 (°)
(*A*)	31.2	4	−38	3	42	1	−41
(*B*)	58.2	6	−26	3	32	3	−29
(*C*)	36.9	5	−31	2	36	3	−33
InP		19.58	−19.88	20.37	39.46	−0.79	−40.25

result. This is a structure-factor-refinement procedure based on the same principles as in the intersecting Kikuchi/HOLZ-line methods discussed in connection with (7).

To further improve the match between experimental and theoretical intensities, additional structure factors were included in the refinement. In general, high-order beams must be included in the calculations to preserve characteristic features in the CBED pattern such as HOLZ lines. However, the corresponding structure-factor amplitudes are not crucial because their effect on the CBED pattern is highly localized. Typical examples in this pattern are the $7\bar{1}1$, $7\bar{1}5$, $9\bar{1}3$ and $9\bar{1}5$ reflections with corresponding HOLZ lines. On the other hand, CBED patterns are sensitive to the coupling between these higher-order beams *via* the 002 and 004 reflections.

Intuitively, one would like to refine the structure factors of all beams included in the calculations (25 in this example). In practice, this is not possible, so our attention was first given to low-order beams (002, 004 and 006). In addition, the $\bar{2}0\bar{6}$ structure factor is considered as it has a major effect on the CBED pattern (notice the thickness fringes parallel to the $\bar{2}0\bar{6}$ HOLZ line). Finally, the 008 beam is at the Bragg position; for symmetry reasons (it is part of the 002 systematics), its structure-factor amplitude U_{008} is refined as well.

Thus, in total the following five beams were refined: 002, 004, 006, 008 and $\bar{2}0\bar{6}$. The fit factor χ_2^2 was minimized with respect to both the incident-beam direction and the corresponding structure-factor amplitudes. For approaches (*B*) and (*C*), as a direct consequence of the initial assumption, all structure-factor phases were fixed to zero. The results of the refinements are summarized in Table 3, the minimized fit factors χ_2^2 are listed in Table 2. The calculations confirm that the initial assumption (*C*) is better than (*B*). Assuming that the refined structure factors found in row (*A*) are accurate, all structure factors in (*C*) are found with an accuracy better than 5%. Using approach (*B*), only the two lowest-order structure factors are found with the same accuracy. The three structure factors of the 006, 008 and $\bar{2}0\bar{6}$ are estimated with an accuracy of only 20%.

6.3. *Refinements of three-phase invariants*

Only small areas of the observed pattern are sensitive to the structure-factor phases, so the pixel-sensitive QCBED method is required. Areas near crossings of strongly coupled high-order reflections are known to be sensitive to three-phase invariants. These areas include the simultaneous three-beam Bragg condition. In the pattern studied, the crossing of the $7\bar{1}3$ and $7\bar{1}5$ HOLZ lines is an ideal area to study the three-phase invariant $\psi_1 = \varphi_{7\bar{1}3} - \varphi_{7\bar{1}5} + \varphi_{002}$. The three-phase invariant $\psi_2 = \varphi_{7\bar{1}3} - \varphi_{7\bar{1}7} + \varphi_{004}$ will be considered as well, since the splitting of the $7\bar{1}3$ and $7\bar{1}7$ HOLZ lines are well defined within the pattern. In the calculations, the 002 phase is equal to zero.

First, the parameter-sensitive areas are identified. The parameters to be refined, *i.e.* the three phases $\varphi_{7\bar{1}3}$, $\varphi_{7\bar{1}5}$ and $\varphi_{7\bar{1}7}$, are given a random initial value of 45° and the QCBED method is applied assuming the previously determined beam direction and structure factors to be fixed. The refined phases and the corresponding three-phase invariants are listed in Table 4. The table shows that individual phases cannot be found in this example. Methods (*A*), (*B*) and (*C*) give relatively similar values of a given phase but these values are all wrong (for InP, the phases are listed in the last row of the table). However, using any of the three assumptions (*A*), (*B*) or (*C*), the three-phase invariants ψ_1 and ψ_2 are found with an accuracy better than 10°. Notice that the results in row (*A*) match the true values within 1 or 2°. Results in row (*C*) are within 6–7°, while results in (*B*) are slightly worse. This is reflected in the minimized χ^2 values and is in accordance with our expectations based on earlier observations. In the table, a third three-phase invariant is listed, $\psi_3 = \varphi_{7\bar{1}5} - \varphi_{7\bar{1}7} + \varphi_{002}$. All three approaches estimate this invariant accurately. This is a surprising result since the 'three-beam Bragg condition' is not satisfied for these three beams in the experimental pattern studied. The result is due to the fact that segments away from the Bragg condition are also dependent on these phases.

7. Conclusions

The results show that the intensity in the experimental centre disc of a convergent-beam pattern is well suited for determination of three-phase structure invariants and structure-factor amplitudes in noncentrosymmetric crystals. The information content in the disc is large provided the optimal intensity details can be extracted. For this purpose, the novel algorithm for parameter-sensitive pixel sampling of experimental intensities has been included in the refinement procedure. This is found to increase the sensitivity of the refinement and reduces the computer time. By use of the standard procedure in the refinement, which use neutral atoms as initial choice,

individual phase invariants were determined with typically 1–2° accuracy while structure-factor amplitudes were better than 0.5%. Even unrealistic starting assumptions and incorrect temperature factors lead to good results for the three-phase structure invariant. This quantity appeared to be stable even for cases where the individual phases were wrong. The reason why individual phases cannot be determined in the present case is that there are no intensity features in the centre disc that can clearly be ascribed to individual phases. The three-beam cases discussed have been tested theoretically for phase-sensitive pixels. We found that there are strong spatial correlations, a result that explains the problem. For sparse zones, the present results show that three-phase invariants can be determined in large numbers from nonsystematic dynamical diffraction effects in CBED patterns. One can easily tilt from zone to zone. The effects are most easily identified in cases with relatively strong coupling reflections as in the present case. Such a procedure can preferentially be coupled to X-ray results as the electron structure factors and structure invariants can easily be transformed to the corresponding X-ray values.

References

Anstis, G. R. (1996). *Acta Cryst.* A**52**, 450–455.

Bethe, H. S. (1928). *Ann. Phys. (Leipzig)*, **87**, 55–69.

Bird, D., James, R. & Preston, A. R. (1987). *Phys. Rev. Lett.* **59**, 1216–1218.

Bird, D. M. & King, Q. A. (1990). *Acta Cryst.* A**46**, 202–208.

Birkeland, C. R., Høier, R., Holmestad, R. & Marthinsen, K. (1997). *Proc. Electron Microscopy and Analysis Group Conf., EMAG-97, Cambridge. Inst. Phys. Conf. Proc.* No. 153, pp. 133–136. Bristol: Institute of Physics.

Birkeland, C. R., Holmestad, R., Marthinsen, K. & Høier, R. (1996). *Ultramicroscopy*, **66**, 89–99.

Blaha, K., Schwarz, P. D. & Augustyn, R. (1990). Updated version of original code. *Wien*95. University of Vienna, Austria.

Blaha, K., Schwarz, P. D., Sorantin, P. & Triskey, S. B. (1990). *Comput. Phys. Commun.* **59**, 399.

Chang, S. L. (1987) *Crystallogr. Rev.* **1**, 87–189.

Cheng, Y. F., Nüchter, W., Mayer, J., Weickenmeier, A. L. & Gjønnes, J. (1996). *Acta Cryst.* A**52**, 923–936.

Dorset, D. L. (1995). *Structural Electron Crystallography*. New York: Plenum Press.

Fox, A. G. & Fisher, R. M. (1988). *Aust. J. Phys.* **41**, 461–474.

Giacovazzo, C. (1980). *Direct Methods in Crystallography*. London: Academic Press.

Gjønnes, J. & Høier, R. (1969). *Acta Cryst.* A**25**, 595–602.

Gjønnes, J. & Høier, R. (1971). *Acta Cryst.* A**27**, 313–316.

Goodman, P. & Lehmpfuhl, G. (1967). *Acta Cryst.* **22**, 14–24.

Hart, M. & Lang, A. R. (1961). *Phys. Rev. Lett.* **7**, 120–121.

Høier, R. (1972). *Phys. Status Solidi A*, **11**, 597–602.

Høier, R. & Aanestad, A. (1981). *Acta Cryst.* A**37**, 787–794.

Høier, R. & Andersson, B. (1974). *Acta Cryst.* A**30**, 93–95.

Høier, R., Bakken, L. N., Marthinsen, K. & Holmestad, R. (1993). *Ultramicroscopy*, **49**, 159–170.

Høier, R. & Marthinsen, K. (1983). *Acta Cryst.* A**39**, 854–860.

Holmestad, R. & Birkeland, C. R. (1998) *Philos. Mag. A.* **77**, 1231–1254.

Holmestad, R., Birkeland, C. R., Marthinsen, K., Høier, R. & Zuo, J. M. (1999). *Microsc. Res. Tech.* In the press.

Holmestad, R., Zuo, J. M., Spence, J. C. H., Høier, R. & Horita, Z. (1995). *Philos. Mag.* A**72**, 579–601.

Hurley, A. C. & Moodie, A. F. (1980). *Acta Cryst.* A**36**, 737–738.

Ichimiya, A. & Uyeda, R. (1977). *Z. Naturforsh. Teil A*, **32**, 750–753.

Kambe, K. (1957). *J. Phys. Soc. Jpn*, **12**, 13–31.

Larsen, H. B. & Thorkildsen, G. (1998). *Acta Cryst.* A**54**, 137–145.

Marthinsen, K., Bakken, L. N., Høier, R. & Runde, P. (1990). *Microbeam Analysis*, pp. 347–350. San Fransisco Press.

Marthinsen, K. & Høier, R. (1986). *Acta Cryst.* A**42**, 484–492.

Marthinsen, K. & Høier, R. (1988). *Acta Cryst.* A**44**, 558–562.

Marthinsen, K., Matsuhata, H., Høier, R. & Gjønnes, J. (1988). *Aust. J. Phys.* **41**, 449–463.

Mathiesen, R. H., Mo, F., Eikenes, A., Nyborg, T. & Larsen, H. B. (1998). *Acta Cryst.* A**54**, 338–347.

Moodie, A. F., Etheridge, J. & Humphreys, C. J. (1996). *Acta Cryst.* A**52**, 596–605.

Nüchter, W., Weickenmeier, A. L. & Mayer, J. (1998). *Phys. Status Solidi A*, **166**, 367–379.

Press, W. H., Flannery, B. P., Teukolsky, S. A. & Vetterling, W. T. (1986). *Numerical Recipes.* New York: Cambridge University Press.

Reid, J. S. (1983). *Acta Cryst.* A**39**, 1–13.

Saunders, M., Bird, D. M., Zaluzec, N. F., Burgess, W. G., Preston, A. R. & Humphreys, C. J. (1995). *Ultramicroscopy*, **60**, 311–323.

Shen, Q. (1998). *Phys. Rev. Lett.* **80**, 3268–3271.

Spence, J. C. H. (1993). *Acta Cryst.* A**49**, 231–260.

Spence, J. C. H. (1998). *Acta Cryst.* A**54**, 7–18.

Spence, J. C. H. & Zuo, J. M. (1992). *Electron Microdiffraction.* New York: Plenum.

Tomokiyo, Y., Matsumura, S., Okuyama, T., Yasunaga, T., Kuwano, N. & Oki, K. (1993). *Ultramicroscopy*, **54**, 276–285.

Watanabe, D., Uyeda, R. & Kogiso, M. (1968). *Acta Cryst.* A**24**, 249–250.

Weckert, E. & Hümmer, K. (1997). *Acta Cryst.* A**53**, 108–143.

Zhu, H. R & Zuo, J. M. (1993). *Ideal Microscope.* EMLab Software, 16203 S. 26th Place, Phoenix, AZ 85048, USA.

Zuo, J. M. (1992). *Ultramicroscopy*, **41**, 211–227.

Zuo, J. M. (1999). *Microsc. Res. Tech.* In the press.

Zuo, J. M., Høier, R. & Spence, J. C. H. (1989). *Acta Cryst.* A**45**, 839–856.

Zuo, J. M., O'Keeffe, M., Rez, P. & Spence, J. C. H. (1997). *Phys. Rev. Lett.* **78**, 4777–4780.

Zuo, J. M., Spence, J. C. H., Downs, J. & Mayer, J. (1993). *Acta Cryst.* A**49**, 422–429.

Zuo, J. M., Spence, J. C. H. & Høier, R. (1989). *Phys. Rev. Lett.* **62**, 547–549.

Zuo, J. M., Spence, J. C. H. & O'Keeffe, M. (1988). *Phys. Rev. Lett.* **61**, 353–356.